Mean-field energies of spin-flux phases

Sajeev John and Axel Müller-Groeling
Department of Physics, University of Toronto, 60 St. George Street, Toronto, Ontario, Canada M5S 1A7
(Received 21 July 1994)

It is suggested that conventional spin-density-wave states for an interacting many-electron system in a two-dimensional square lattice are energetically unstable to the formation of spin flux. Spin flux corresponds to a rotation of the *internal* coordinate system of the electron as it traverses a closed loop. The flux is dynamically generated by the electromagnetic interaction in the many-body system. This is illustrated by including the nearest-neighbor Coulomb repulsion between electrons in the Hubbard model. Using a Grassmann field theory, we derive the mean-field equations for spin flux and local-moment ordering. For a wide range of Hubbard model couplings U/t and doping δ we find that the generation of spin flux leads to a lowering of the mean-field local-moment amplitude. This suppression of the local moment offsets the additional quantum zero-point energy associated with spin flux and leads to an overall reduction in the total many-electron energy. When the spin-flux vortex filaments are endowed with a quantum dynamics, chiral symmetry breaking is possible. We show that under certain conditions, this leads to a further reduction of local-moment amplitude and many-electron energy.

I. INTRODUCTION

The understanding of doped Mott insulators is a fundamental problem in condensed-matter physics.[1] Considerable attention has been focused on this problem, due to the suggestion by Anderson[2] that the high T_c superconducting cuprates[3] exhibit unconventional metallic behavior as a result of the crossover from Mott insulating behavior to Fermi-liquid behavior as a function of doping. These systems possess local spin-$\frac{1}{2}$ magnetic moments, which exhibit magnetic long-range order and a Mott-Hubbard charge-transfer gap at small doping. At intermediate doping values corresponding to high-temperature superconductivity, magnetic long-range order is destroyed by fluctuation effects and the Mott-Hubbard charge transfer gap exhibits a variety of subgap electronic structure at infrared frequencies.[4–7] It is our hypothesis that the non-Fermi-liquid behavior of the metallic state at intermediate doping[8,9] is the result of an interplay between electronic degrees of freedom and the remnant, collective modes of the spin-$\frac{1}{2}$ magnetic background.

In some recent papers,[10,11] the concept of *spin flux* was introduced. We recapitulate the main arguments given there to keep this paper self-contained. In Refs. 10 and 11, spin flux was interpreted to originate from a fundamental extension of the physical Hilbert space for interacting, spin-$\frac{1}{2}$ electrons. The extension consisted of the hypothesis that the many-electron wave function can exhibit antiperiodicity when the electron coordinate circulates around a closed loop encircling certain isolated singularities. This is analogous to, but entirely distinct from the wave-function symmetry in the presence of an isolated magnetic vortex-line singularity, which contains a magnetic π flux. Flux phases exhibiting conventional U(1) magnetic flux have been studied widely in the recent literature.[12–16] The spin-flux phase is distinct from these U(1) flux phases in that there is no measurable magnetic field associated with the wave-function singularity.

Instead, the singularity was interpreted[10,11] to be an *intrinsic* property of the many-electron wave function. The picture used to visualize this property is reproduced in Fig. 1. The many-electron wave function may be regarded (in a variational sense) as a Slater determinant of one-electron wave functions, each having a *Möbius strip* character: Associate one value, χ, of the wave function with one side of the strip and the other value, $-\chi$, with the other side of the strip. As the electron encircles a closed loop, the wave function switches continuously from one value to the other.

This twist of the electronic spinor wave function as it encircles a closed path may be formally described by the introduction of an SU(2) "gauge" field in the many-electron Hamiltonian. That is to say, the hopping matrix element from site i to site j is given by the product of an amplitude, t, and an SU(2) matrix,

$$T^{ij} = \exp\left[\frac{i}{2}\int_i^j d\mathbf{l}\cdot\mathbf{A}^k\sigma^k\right]. \tag{1.1}$$

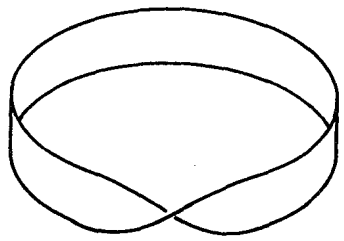

FIG. 1. The Möbius strip topology of the two-valued electron spinor wave function, as it encircles a closed path in coordinate space.

Here, σ^k, $k=1,2,3$, are the 2×2 Pauli spin matrices. The $\mathbf{A}^k$, $k=1,2,3$, are the three components of the "gauge" field, which is circulation free, except for isolated line singularities in three dimensions (point singularities in two dimensions). These singularities have to carry an integer multiple of π flux if they are to describe the Möbius strip topology explained above. In other words, the product of SU(2) matrices around any closed loop is

$$\prod_{\text{closed loop}} (T^{ij})=\pm1 \ . \tag{1.2}$$

When this product is equal to $+1$, the SU(2) matrices can be removed by a unitary "gauge" transformation. This corresponds to a homotopically trivial spin rotation of the electron's internal coordinate system at different lattice points. When the product is equal to -1, this corresponds to the presence of a flux singularity enclosed by the loop. This singularity cannot be removed by a unitary transformation and describes the extension of the physical Hilbert space to include the antiperiodic spin-$\frac{1}{2}$ wave functions postulated in Refs. 10 and 11.

In the technical framework discussed so far, spin flux is strictly quantized in integer units of π from a microscopic point of view. This is a direct consequence of the two valuedness of spin-$\frac{1}{2}$ wave functions and the doubly connected topology of the rotation group manifold SO(3), leading to either the usual (periodic) or the Möbius strip topology. However, if one assumes that vortexline filaments of spin flux can exhibit quantum-mechanical motion through the many-electron system, the quantum-mechanical *expectation value* of spin flux may differ from its eigenvalues. In this way, arbitrary flux values between 0 and π could be realized.

Having rephrased the original arguments in Refs. 10 and 11 we now proceed to discuss spin flux from a formal point of view. We demonstrate that spin flux can arise in the framework of mean-field theory for a system of many electrons interacting via electromagnetic forces. To show this, we generalize the Hubbard model by retaining the Coulomb repulsion between electrons on neighboring sites. Consider the Hamiltonian,

$$\mathcal{H}=-t_0\sum_{\langle ij\rangle,\alpha}(c^\dagger_{i\alpha}c_{j\alpha}+\text{H.c.})+U\sum_i n_{i\uparrow}n_{i\downarrow}+V\sum_{\langle ij\rangle}n_in_j \ . \tag{1.3}$$

Here, $c^\dagger_{i\alpha}$ is the creation operator for an electron of spin α at site i, t_0 the bare nearest-neighbor hopping matrix element, U the on-site Coulomb repulsion, and V the nearest-neighbor Coulomb repulsion. Also, $n_i=c^\dagger_{i\uparrow}c_{i\uparrow}+c^\dagger_{i\downarrow}c_{i\downarrow}$. A spin-flux mean-field factorization of the nearest-neighbor Coulomb repulsion term follows by writing the product,

$$n_in_j=2n_i-\sum_{\alpha\beta}(c^\dagger_{i\alpha}c_{j\beta})(c^\dagger_{i\alpha}c_{j\beta})^\dagger \tag{1.4}$$

$$=2n_i-\tfrac{1}{2}\sum_{\mu=0}^{3}S^\mu_{ij}(S^\mu_{ij})^\dagger \ , \tag{1.5}$$

where $S^\mu_{ij}=\sum_{\alpha\beta}c^\dagger_{i\alpha}\sigma^\mu_{\alpha\beta}c_{j\beta}$. Here, σ^0 is the 2×2 identity matrix and σ^k, $k=1,2,3$, are the Pauli spin matrices. Equation (1.4) follows directly from the anticommutation algebra of the electron operators and Eq. (1.5) follows from the Pauli matrix identity:

$$\tfrac{1}{2}\sum_{\mu=0}^{3}\sigma^\mu_{\alpha\beta}(\sigma^\mu_{\alpha'\beta'})^*=\delta_{\alpha\alpha'}\delta_{\beta\beta'} \ . \tag{1.6}$$

In the Hartree-Fock approximation, we replace the operator product $S^\mu_{ij}(S^\mu_{ij})^\dagger$ by the expression $\langle S^\mu_{ij}\rangle_0(S^\mu_{ij})^\dagger+S^\mu_{ij}\langle(S^\mu_{ij})^\dagger\rangle_0-\langle S^\mu_{ij}\rangle_0\langle(S^\mu_{ij})^\dagger\rangle_0$. The four-component vector,

$$\langle\mathbf{S}_{ij}\rangle_0=\frac{2t_0}{V}(\chi_{ij},i\Delta_{ij}\hat{n}_{ij}) \ , \tag{1.7}$$

describes the quantum-mechanical expectation value, where the amplitudes χ_{ij} and Δ_{ij} associated with a given link are to be determined self-consistently in Hartree-Fock theory. The symbol $\hat{n}_{ij}$ denotes a three-dimensional unit vector. The amplitudes χ_{ij} and Δ_{ij} correspond to the presence of charge and spin currents, respectively, on the link $\langle ij\rangle$. Suppose for simplicity that $\chi_{ij}=0$, $|\Delta_{ij}|=\Delta$, and $\hat{n}_{ij}=\hat{n}$ for all $\langle ij\rangle$. Then the mean-field Hamiltonian is given by

$$\mathcal{H}_{\text{MF}}=-t\sum_{\langle ij\rangle,\alpha\beta}(c^\dagger_{i\alpha}T^{ij}_{\alpha\beta}c_{j\beta}+\text{H.c.})$$
$$+U\sum_i n_{i\uparrow}n_{i\downarrow}+VN_{\text{op}}z+4\frac{t_0^2}{V}\Delta^2L \ . \tag{1.8}$$

Here, $T^{ij}_{\alpha\beta}=(\delta_{\alpha\beta}+i\Delta_{ij}\hat{n}\cdot\sigma_{\alpha\beta})/\sqrt{1+\Delta^2}$, $t=t_0\sqrt{1+\Delta^2}$, $N_{\text{op}}=\sum_i n_i$, and L is the total number of links on the lattice. In a discussion of an itinerant Heisenberg model in Ref. 17, a trial Hamiltonian similar to the mean-field Hamiltonian derived here was employed and studied by means of group-theoretical methods.

The conventional Hubbard model may be regarded as a choice of mean-field amplitudes Δ_{ij}, for which the product of SU(2) matrices $T^{ij}_{\alpha\beta}$ around *every* elementary plaquette of the lattice is given by the identity matrix. A spin-flux state corresponds to a mean field in which this product is allowed to deviate from unity. Our derivation suggests the following interpretation: Spin flux is dynamically generated by the fact that the electrons experience an effective spin-dependent interaction originating from the collective background. It is this interaction that affects the electron's spin rotation and leads to a nontrivial flux value. The relation to U(1) flux phases discussed earlier[12–16] becomes particularly transparent now: While U(1) flux phases arise from a mean-field approximation, where the single-particle Hamiltonian contains the analog of a magnetic field (one could call this a *unitary* model), the spin-flux phase corresponds to a single-particle approximation containing the analog of a spin-orbit term (a *symplectic* model).

This formal mean-field theory of spin flux is completely general: While this approach can certainly describe a π spin-flux phase, it does not attribute a special significance to this particular value. The quantization of spin flux following from the original interpretation[10,11] (or the absence thereof) must be tested experimentally. One possible test is through the measurement of *discrete* subgap electronic levels induced by solitons. We do not address

this question in this paper. Instead, we focus attention on more general consequences of nonvanishing spin flux.

In this paper, we present a comparison of the mean-field energies of the doped, antiferromagnetic Mott insulators with and without the presence of spin flux. We find that the presence of spin flux leads to a reduction in the magnitude of local magnetic moments and the resulting Mott-Hubbard charge gap. This in turn leads to a lowering of the many-electron Hartree-Fock energy in the two-dimensional square lattice. For the purpose of illustration, we compare two limiting cases only. In the first case, we allow a spin flux of $\pm\pi$ to penetrate each plaquette of the square lattice. This is compared to the case in which spin flux is absent. A self-consistent determination of the spin-current amplitude, Δ_{ij}, and the possibility of general spin-flux mean fields as a function of doping will be discussed elsewhere. A simple extension of the π-flux state to incorporate next-nearest-neighbor hopping and chiral-symmetry breaking is described.

II. MEAN-FIELD THEORY INCLUDING SPIN FLUX

We consider a generalized Hubbard Hamiltonian on a square lattice,

$$\mathcal{H}=-t\sum_{\langle ij\rangle}\psi_i^\dagger T^{ij}\psi_j+U\sum_i n_{i\uparrow}n_{i\downarrow}\ , \tag{2.1}$$

where $\psi_i^\dagger=(c_{i\uparrow}^\dagger,c_{i\downarrow}^\dagger)$ is a two component creation operator, $\langle ij\rangle$ denotes the sum over nearest-neighbor pairs of sites, and $T^{ij}\in$SU(2). We emphasize that the Hamiltonian Eq. (2.1) is derived from the generalized Hubbard model. As explained in the introduction, it takes into account the nearest-neighbor interaction in that T^{ij} can deviate from unity. We will consider the case where the matrix product of T^{ij} is equal to -1. The partition function of this model can be written as a functional integral involving Grassmann variables,

$$Z=\frac{1}{N}\int d[\psi^\dagger,\psi]\exp\left\{-\int_0^\beta d\tau\sum_i\psi_i^\dagger(\partial_\tau-\mu_0)\psi_i-\int_0^\beta d\tau H(\psi_i^\dagger,\psi_i)\right\}. \tag{2.2}$$

The electron operators in the Hamiltonian Eq. (2.2) are replaced by Grassmann numbers (without changing the notation). To develop the formal framework of our investigation, we consider a staggered spin-flux pattern in this section. We consider a regular lattice of plaquettes [containing four sites $1,\ldots,4$, see Fig. 2(a)], where adjacent plaquettes are threaded by a spin flux of opposite sign, but the same absolute value π. Obviously, this construction does not uniquely specify the T^{ij}. Instead, there are infinitely many possibilities to realize this situation by prescribing particular values for the T^{ij}, all of them being connected by "gauge" transformations,

$$\begin{aligned}&\psi\to\psi'=U\psi\ ,\\&T\to T'=UTU^\dagger;\ \ [U\in\mathrm{SU}(2)]\ .\end{aligned} \tag{2.3}$$

In what follows we will adopt the simplest possible "gauge", where all T^{ij} are equal to unity, except those which connect sites 1 and 2 [see Fig. 2(a)]: These are equal to -1.

We proceed to derive a mean-field expression for the partition function Eq. (2.2). Since $(\psi_i^\dagger\psi_i)^2=2n_{i\uparrow}n_{i\downarrow}$ and $(\psi_i^\dagger\sigma\psi_i)^2=-6n_{i\uparrow}n_{i\downarrow}$ [where $\sigma=(\sigma_x,\sigma_y,\sigma_z)$ denotes the Pauli spin matrices], the Hubbard-Stratonovitch transformation can be written as

$$\exp\left\{-\int_0^\beta d\tau\,U\sum_i n_{i\uparrow}n_{i\downarrow}\right\}=\frac{1}{N'}\int d[\phi^a,\rho]\exp\left\{-\int_0^\beta d\tau\sum_i\left[\rho_i^2+\sum_a\phi_i^a\phi_i^a+\alpha\rho_i\psi_i^\dagger\psi_i+\gamma\sum_a\phi_i^a(\psi_i^\dagger\sigma_a\psi_i)\right]\right\}. \tag{2.4}$$

Here, α and γ are two parameters constrained by the requirement that $3\gamma^2-\alpha^2=2U$ and ρ_i and ϕ_i^a $(a=1,2,3)$ are decoupling (or order parameter) fields. The lattice Fourier transform is introduced by $\psi_i(\tau)=L^{-1/2}\sum_{kn}\exp(i\mathbf{k}\mathbf{r}_i-\omega_n\tau)\psi_{kn}$ and plaquette quantities are denoted by a hat. E.g., $\hat\psi$ is an eight-component vector with entries $(\psi^{(1)},\psi^{(2)},\psi^{(3)},\psi^{(4)})$ and $\hat\rho$ is a direct product of the identity in spin space and a 4×4 diagonal matrix with entries $(\rho^{(1)},\rho^{(2)},\rho^{(3)},\rho^{(4)})$. The superscripts correspond to the lattice sites within a given plaquette. With this notation, we get

$$Z=\frac{1}{N}\int d[\psi^\dagger,\psi,\phi^a,\rho]\exp\left\{-\beta UL\sum_{kn}\mathrm{tr}\left[\hat\rho_{kn}^*\hat\rho_{kn}+\sum_a\hat\phi_{kn}^{*a}\hat\phi_{kn}^a\right]+\beta\sum_{kn}\hat\psi_{kn}^\dagger[i\omega_n+\mu_0-A_x(k)-A_y(k)]\hat\psi_{kn}\right.$$
$$\left.-\beta U\sum_{knk'n'}\hat\psi_{kn}^\dagger(\alpha\hat\rho_{k-k',n-n'}+\gamma\hat\phi_{k-k',n-n'}^a\sigma_a)\hat\psi_{k'n'}\right\}. \tag{2.5}$$

Setting the lattice spacing to unity all momentum summations range over the reduced Brillouin zone k_x, $k_y\in[-\pi/2,\pi/2]$ and L denotes the number of *plaquettes* constituting the lattice. Furthermore, in deriving Eq. (2.5), we have rescaled

$$\begin{aligned}&\alpha\to\alpha'=\alpha/\sqrt{U},\ \ \gamma\to\gamma'=\gamma/\sqrt{U}\ ,\\&\phi_{kn}^a\to\phi_{kn}^{a'}=\phi_{kn}^a/\sqrt{UL},\ \ \rho_{kn}\to\rho'_{kn}=\rho_{kn}/\sqrt{UL}\end{aligned} \tag{2.6}$$

and omitted the primes thereafter so that the constraint on γ and α now reads $3\gamma^2-\alpha^2=2$. Finally, $A_x(k)$ and $A_y(k)$

are direct products of 4×4 matrices (determined by the plaquette-internal structure and the lattice dispersion relation) with the identity in spin space,

$$A_x(k)=-2t\cos(k_x)\alpha_x=-2t\cos(k_x)\begin{bmatrix}-\tau_x & 0\\ 0 & \tau_x\end{bmatrix}=-2t\cos(k_x)(-\gamma_z\tau_x)\,,$$
$$A_y(k)=-2t\cos(k_y)\alpha_y=-2t\cos(k_y)\begin{bmatrix}0 & \tau_x\\ \tau_x & 0\end{bmatrix}=-2t\cos(k_y)(\gamma_x\tau_x)\,. \tag{2.7}$$

Here, we have introduced the following notation: $\gamma_{x,y,z}$ and $\tau_{x,y,z}$ denote Pauli matrices defined in subspaces of the 4×4 plaquette-internal space, corresponding to the upper/lower and left/right parts of the plaquette, respectively, see Fig. 2(a). We have suppressed the tensor product symbol $\otimes$ for simplicity. The specific form of A_x and A_y in Eq. (2.7) is due to the "gauge" [the particular values of the T^{ij} in Eq. (2.1)] chosen; however, the fact that A_x and A_y anticommute is of course independent of this choice. Integrating over the Grassmann variables in Eq. (2.5) and distinguishing operators from their components entering Eq. (2.5) by a tilde, we arrive at

$$\frac{1}{N}\int d[\rho,\phi^a]\exp\left\{-\beta UL\sum_{kn}\mathrm{tr}\left[\hat{\rho}^*_{kn}\hat{\rho}_{kn}+\sum_a\hat{\phi}^{a*}_{kn}\hat{\phi}^a_{kn}\right]\right.$$
$$\left.+\mathrm{tr}\ln\left[-\beta[i\tilde{\omega}+\tilde{\mu}_0-\tilde{A}_x-\tilde{A}_y]+\beta U\left[\alpha\tilde{\rho}+\gamma\sum_a\tilde{\phi}^a\sigma_a\right]\right]\right\}. \tag{2.8}$$

Eq. (2.8) is still rigorously equivalent to Eq. (2.2).

To reduce the unmanageable complexity of Eq. (2.8), we choose common and physically plausible, time-independent "mean-field" forms for the decoupling fields. In this way, only a few parameters enter the problem, which can later be determined from a stationarity (or saddle-point) condition. Note that this is a mean-field treatment of the *onsite* interaction, which should not be confused with the mean-field theory for the nearest-neighbor interaction derived in Sec. I. The mean-field theory for the nearest-neighbor Coulomb interaction is already contained in the structure of the matrices $\tilde{A}_x$ and $\tilde{A}_y$. In a more general theory, the spin-flux itself would need to be determined self-consistently. It has recently been shown by Lieb[18] that for one electron per site ($\delta=0$), the π-spin-flux state has the lowest energy for any given choice of the other parameters. For $\delta>0$, it is possible that the self-consistently determined average spin flux per plaquette may deviate from π. This would lead to self-consistency equations for $\tilde{A}_x$ and $\tilde{A}_y$. We leave the problem of generalized spin flux for future work. By fixing the spin-flux mean field to π, only few self-consistent parameters enter the problem.

The mean-field expressions for the onsite decoupling fields, denoted by a bar, are best defined in coordinate space:

$$\overline{\rho_i}=\rho_0=\mathrm{const}$$
$$\overline{\phi^a_i\sigma_a}=\begin{bmatrix}\overline{\phi^z_i} & \overline{\phi^x_i-i\phi^y_i}\\ \overline{\phi^x_i+i\phi^y_i} & -\overline{\phi^z_i}\end{bmatrix}, \tag{2.9}$$

where $\overline{\phi^z_j}=0$ ($j=1,\ldots,4$ is a site index for a given plaquette) and

$$\overline{\phi^x_1-i\phi^y_1}=S\exp(i\mathbf{Q}\cdot\mathbf{r})\,,$$
$$\overline{\phi^x_2-i\phi^y_2}=S\exp[i\mathbf{Q}\cdot(\mathbf{r}+\mathbf{e}_x)]\,,$$
$$\overline{\phi^x_3-i\phi^y_3}=S\exp[i\mathbf{Q}\cdot(\mathbf{r}+\mathbf{e}_x+\mathbf{e}_y)]\,, \tag{2.10}$$
$$\overline{\phi^x_4-i\phi^y_4}=S\exp[i\mathbf{Q}\cdot(\mathbf{r}+\mathbf{e}_y)]\,.$$

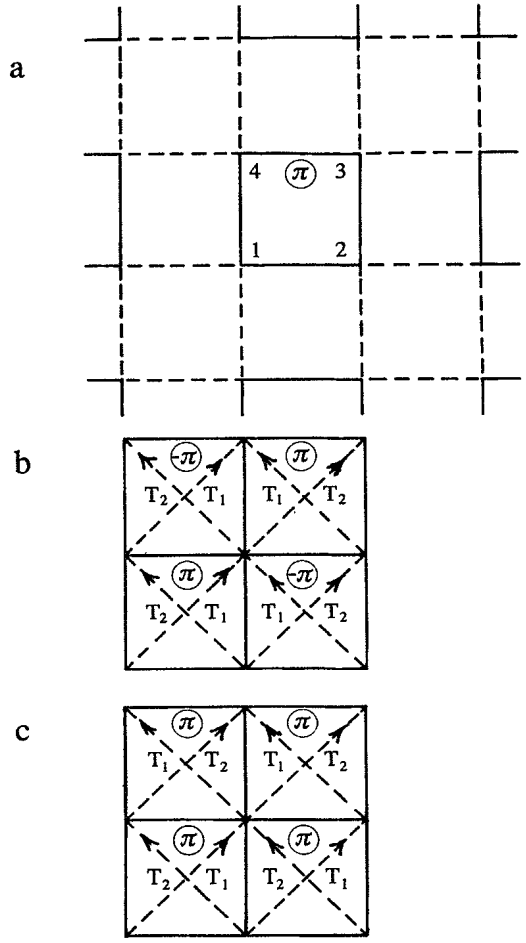

FIG. 2. (a) Numbering of the sites inside a plaquette. The plaquette is threaded by spin flux $+\pi$. (b) Our convention for next-nearest-neighbor hopping amplitudes in the staggered spin-flux configuration. Thick lines correspond to $-t$, thin lines to $+t$, $T_1=it_{\mathrm{nnn}}\sigma_z$, and $T_2=-it_{\mathrm{nnn}}\sigma_z$. (c) Our convention for next-nearest-neighbor hopping amplitudes in the homogeneous spin-flux configuration. Thick lines correspond to $-t$, thin lines to $+t$, $T_1=it_{\mathrm{nnn}}\sigma_z$, and $T_2=-it_{\mathrm{nnn}}\sigma_z$.

Here, r is the location of site 1 of the plaquette in question, $\mathbf{Q}=(Q_x,Q_y)$ is a two-dimensional vector with $Q_x,Q_y\in[0,\pi]$ and $\mathbf{e}_x,\mathbf{e}_y$ are unit vectors in x and y directions, respectively. Equations (2.9) and (2.10) describe a mean-field spiral background state with homogeneous charge distribution. The spiral state is parametrized by the mean-field magnetization S and the "spiral pitch" Q. Obviously, the spiral background has a single nonvanishing Fourier component (Q) and couples only spin-up fields with spin-down fields. Since the location of the Brillouin zone is at our disposal, we can shift the argument of, say, the spin-up components [cf. Eq. (2.5)] by Q and thus group exactly those two field components together, which are coupled by the spiral background. Omitting the discussion of rather subtle sign changes occurring during the rigorous implementation of this scheme, the result of our efforts to simplify the problem can be summarized as follows. The partition function in the mean-field approximation is given by

$$Z=\exp(-S_{\text{eff}})=\exp\{-\beta UL\,(4\rho_0^2+4S^2) +\operatorname{tr}\ln(-\beta[i\tilde{\omega}+\tilde{\mu}-\tilde{H}_{\text{MF}}])\}\ , \tag{2.11}$$

with

$$(\tilde{H}_{\text{MF}})_{k,n}=\begin{bmatrix} p_x'\alpha_x+p_y'\alpha_y & \gamma US \\ \gamma US & p_x\alpha_x+p_y\alpha_y \end{bmatrix} \tag{2.12}$$

and

$$\begin{aligned} &\tilde{\mu}=\tilde{\mu}_0-\alpha U\rho_0\ , \\ &p_x=-2t\cos(k_x),\quad p_x'=-2t\cos(k_x+Q_x)\ , \\ &p_y=-2t\cos(k_y),\quad p_y'=-2t\cos(k_y+Q_y)\ . \end{aligned} \tag{2.13}$$

$\tilde{H}_{\text{MF}}$ is an 8×8 matrix in spin and site space. We wish to diagonalize $\tilde{H}_{\text{MF}}$ with respect to the remaining nondiagonal entries. The eigenvalues are given by the poles of $\det[(\tilde{H}_{\text{MF}}-E)^{-1}]$. Due to the specific structure of $\tilde{H}_{\text{MF}}$, it is particularly simple to determine those terms which can give rise to singularities in the determinant. Let us denote the (1,1) block of $(\tilde{H}_{\text{MF}}-E)^{-1}$ by X_{11}. Then,

$$\begin{aligned} X_{11}&=[p_x'\alpha_x+p_y'\alpha_y-E-(\gamma US)^2(p_x\alpha_x+p_y\alpha_y-E)^{-1}] \\ &=\{[p_x\alpha_x+p_y\alpha_y-E]^{-1} \\ &\quad\times[(p_x\alpha_x+p_y\alpha_y-E)(p_x'\alpha_x+p_y'\alpha_y-E) \\ &\quad-(\gamma US)^2]\}^{-1}\ . \end{aligned} \tag{2.14}$$

Singularities can only reside in

$$\begin{aligned} X_{11}'&=[(p_x\alpha_x+p_y\alpha_y-E)(p_x'\alpha_x+p_y'\alpha_y-E)-(\gamma US)^2]^{-1} \\ &=[p_xp_x'+p_yp_y'+E^2-(Ep_x+Ep_x')\alpha_x \\ &\quad-(Ep_y+Ep_y')\alpha_y \\ &\quad+(p_xp_y'-p_yp_x')\alpha_x\alpha_y-(\gamma US)^2]^{-1}\ . \end{aligned} \tag{2.15}$$

Multiplying the matrix in square brackets by

$$-p_xp_x'-p_yp_y'-E^2-(Ep_x+Ep_x')\alpha_x-(Ep_y+Ep_y')\alpha_y +(p_xp_y'-p_yp_x')\alpha_x\alpha_y+(\gamma US)^2 \tag{2.16}$$

gives a result proportional to the unit matrix, the factor of proportionality being

$$(Ep_x+Ep_x')^2+(Ep_y+Ep_y')^2-(p_xp_y'-p_yp_x')^2 -[p_xp_x'+p_yp_y'+E^2-(\gamma US)^2]^2\ . \tag{2.17}$$

Therefore, the inverse of $\tilde{H}_{\text{MF}}-E$ does not exist (is singular) whenever

$$E^4-2E^2[(p_x+p_x')^2/2+(p_y+p_y')^2/2-p_xp_x'-p_yp_y'+(\gamma US)^2]+(p_xp_y'-p_yp_x')^2+[p_xp_x'+p_yp_y'-(\gamma US)^2]^2=0\ . \tag{2.18}$$

The solutions of this biquadratic equation are the desired eigenvalues and are given by

$$E_{\pm}^2=\tfrac{1}{2}(\mathbf{p}^2+\mathbf{p}'^2)+(\gamma US)^2\pm\sqrt{\tfrac{1}{4}(\mathbf{p}^2-\mathbf{p}'^2)^2+(\gamma US)^2(\mathbf{p}+\mathbf{p}')^2}\ , \tag{2.19}$$

where $\mathbf{p}=(p_x,p_y)$ and $\mathbf{p}'=(p_x',p_y')$. We conclude that $\tilde{H}_{MF}$ has four different, doubly degenerate eigenvalues, which are symmetric with respect to interchanging primed and unprimed variables. They will be denoted by E_{++}, E_{+-}, E_{-+}, and E_{--}, respectively. In terms of these eigenvalues, the effective mean-field action S_{eff} defined in Eq. (2.11) is given by

$$-S_{\text{eff}}=-4\beta UL(\rho_0^2+S^2)+2\sum_{kn}\ln[\beta^4(i\omega_n+\mu-E_{++})(i\omega_n+\mu-E_{+-})(i\omega_n+\mu-E_{-+})(i\omega_n+\mu-E_{--})]\ . \tag{2.20}$$

Let us define the thermodynamic potential by $\Omega=S_{\text{eff}}/\beta$. Then the mean-field energy of the system is given by $E=\partial\Omega^s/\partial s|_{s=1}$, where Ω^s is the thermodynamic potential corresponding to $s\mathcal{H}$ [instead of $\mathcal{H}$, the original Hamiltonian Eq. (2.1)]. For the effective action in Eq. (2.21), we get

$$E=\left.\frac{\partial\Omega^s}{\partial s}\right|_{s=1}=4UL(\rho_0^2+S^2) -\frac{2}{\beta}\sum_{kn}\frac{(E_{++}+\alpha U\rho_0)(E_{+-}-i\omega_n-\mu)(E_{-+}-i\omega_n-\mu)E_{--}-i\omega_n-\mu)+\cdots}{(i\omega_n+\mu-E_{++})(i\omega_n+\mu-E_{+-})(i\omega_n+\mu-E_{-+})(i\omega_n+\mu-E_{--})}\ , \tag{2.21}$$

where the dots in the numerator indicate three terms originating from cyclic permutations of E_{++}, E_{+-}, E_{-+}, E_{--}.

Performing the Matsubara sums, we arrive at

$$E=4UL(\rho^2+S^2)+2\sum_k (f_k^{++}E_{++}+f_k^{+-}E_{+-}+f_k^{-+}E_{-+}+f_k^{--}E_{--})$$
$$+2\alpha U\rho_0\sum_k (f_k^{++}+f_k^{+-}+f_k^{-+}+f_k^{--}), \tag{2.22}$$

with $f_k^{ss'}=\{\exp[\beta(E_{ss'}-\mu)]+1\}^{-1}$ the Fermi function.

It remains to determine the appropriate values of S and ρ_0 from the saddle-point equations $\partial\Omega/\partial s=0$, $\partial\Omega/\rho_0=0$, and to related ρ_0 to the doping parameter δ. Straightforward calculations show that

$$0=\frac{\partial\Omega}{\partial\rho_0}=8UL\rho_0+2\alpha U\sum_k (f_k^{++}+f_k^{+-}+f_k^{-+}+f_k^{--})$$
$$\Longleftrightarrow \rho_0=-\frac{\alpha}{4L}\sum_k (f_k^{++}+f_k^{+-}+f_k^{-+}+f_k^{--}) \tag{2.23}$$

and for the total number of electrons N,

$$N=4L(1-\delta)=-\frac{\partial\Omega}{\partial\mu}=2\sum_k (f_k^{++}+f_k^{+-}+f_k^{-+}+f_k^{--}). \tag{2.24}$$

Hence,

$$\rho_0=-\frac{\alpha}{2}(1-\delta). \tag{2.25}$$

Furthermore, the second saddle-point equation gives

$$0=\frac{\partial\Omega}{\partial S}=8ULS+2\sum_k \left[f_k^{++}\frac{\partial E_{++}}{\partial S}+f_k^{+-}\frac{\partial E_{+-}}{\partial S}+f_k^{-+}\frac{\partial E_{-+}}{\partial S}+f_k^{--}\frac{\partial E_{--}}{\partial S}\right]$$
$$\Longleftrightarrow 1=-\frac{\gamma U}{2L}\sum_k \left[\frac{f_k^{++}}{2E_{++}}+\frac{f_k^{+-}}{2E_{+-}}+\frac{f_k^{-+}}{2E_{-+}}+\frac{f_k^{--}}{2E_{--}}\right.$$
$$\left.+\frac{(\mathbf{p}+\mathbf{p}')^2}{E_{++}^2-E_{+-}^2}\left[\frac{f_k^{++}}{2E_{++}}-\frac{f_k^{+-}}{2E_{+-}}-\frac{f_k^{-+}}{2E_{-+}}+\frac{f_k^{--}}{2E_{--}}\right]\right]. \tag{2.26}$$

Collecting and combining the results in Eqs. (2.22), (2.23), (2.25), (2.26) and introducing the continuum approximation by means of the substitution $\sum_k\to(L/\pi^2)\int d^2k$, we finally derive the following expression for the mean-field energy per site,

$$\frac{E}{4L}=\frac{1}{2\pi^2}\int_{-\pi/2}^{\pi/2} d^2k\,(f_k^{++}E_{++}+f_k^{+-}E_{+-}+f_k^{-+}E_{-+}+f_k^{--}E_{--})+US^2-\frac{U}{4}\alpha^2(1-\delta)^2, \tag{2.27}$$

while the saddle-point equations read

$$1-\delta=\frac{1}{2\pi^2}\int_{-\pi/2}^{\pi/2} d^2k(f_k^{++}+f_k^{+-}+f_k^{-+}+f_k^{--}) \tag{2.28}$$

and

$$1=-\frac{\gamma U}{2\pi^2}\int_{-\pi/2}^{\pi/2} d^2k\left[\frac{f_k^{++}}{2E_{++}}+\frac{f_k^{+-}}{2E_{+-}}+\frac{f_k^{-+}}{2E_{-+}}+\frac{f_k^{--}}{2E_{--}}+\frac{(\mathbf{p}+\mathbf{p}')^2}{E_{++}^2-E_{+-}^2}\left[\frac{f_k^{++}}{2E_{++}}-\frac{f_k^{+-}}{2E_{+-}}\right.\right.$$
$$\left.\left.-\frac{f_k^{-+}}{2E_{-+}}+\frac{f_k^{--}}{2E_{--}}\right]\right]. \tag{2.29}$$

The choice $\gamma=\alpha=1$ corresponds to the usual Hartree-Fock approximation. The results reported in this paper are based on a numerical evaluation of Eqs. (2.27), (2.28), and (2.29).

III. NUMERICAL RESULTS

In principle, we have to minimize the expression for the energy E, Eq. (2.27), with respect to the parameters Q_x, Q_y, S defining the spiral background, subject to the constraint that μ yields the correct particle number in the system (which is in turn determined by the doping parameter δ). We proceed as follows: For fixed doping δ, Hubbard parameters U/t, and at zero temperature, the mean-field magnetization S and the chemical potential μ are determined by numerically solving the (coupled) saddle-point equations (2.28) and (2.29). With these

values, the mean-field energy Eq. (2.27) is calculated for Q values, defined on a 10×10 mesh in the region $[0,\pi]\times[0,\pi]$. The minimum of these 100 energy values is then accepted as the mean-field energy of the phase at the given particular values of the parameters. In some cases, finding a stable solution of the saddle-point equations turned out to be cumbersome and we changed our procedure. Fixing Q_x, Q_y, and S, the chemical potential was calculated from Eq. (2.28) and a subsequent search in the remaining three-dimensional parameter space then identified the energy minimum. This latter algorithm, disregarding entirely the information from the second saddle-point equation (2.29), proved to be more reliable but certainly less efficient than the first scheme.

For the parameters α and γ entering the Hubbard-Stratonovitch transformation, we chose $\alpha=\gamma=1$. This choice is the usual one in the sense that in this case, the mean-field description following from Eqs. (2.27)–(2.29) corresponds to a Hartree-Fock treatment employing the equation of motion method. Furthermore, we neglect the third term in Eq. (2.27) in the sequel. For given U and δ, it is just a constant and, therefore, irrelevant for our considerations.

The main purpose of the present paper is to investigate whether or not the spin-flux phase proposed in Refs. 10 and 11 has an energetic advantage as compared to the usual spin-density wave. In Ref. 19, the properties of the spin-density wave were discussed in great detail, using essentially the same theoretical framework as the one employed in the last section. From Ref. 19, the mean-field equations corresponding to our Eqs. (2.27)–(2.29) for the case of the spin-density wave read (the number of sites being $4L$)

$$\frac{E}{4L}=\frac{1}{4\pi^2}\int_{-\pi}^{\pi}d^2k(f_k^+E_+ +f_k^-E_-)+US^2\,, \tag{3.1}$$

$$1-\delta=\frac{1}{4\pi^2}\int_{-\pi}^{\pi}d^2k(f_k^+ +f_k^-)\,, \tag{3.2}$$

$$1=-\frac{U}{4\pi^2}\int_{-\pi}^{\pi}d^2k\left[\frac{f_k^+-f_k^-}{E_+-E_-}\right], \tag{3.3}$$

with

$$E_\pm=\tfrac{1}{2}(\epsilon_k+\epsilon_{k+Q})\pm\tfrac{1}{2}\sqrt{(\epsilon_k-\epsilon_{k+Q})^2+4(US)^2}\,, \tag{3.4}$$

where $\epsilon_k=-2t(\cos k_x+\cos k_y)$. Our first task is to compare the energy values resulting from Eqs. (3.1)–(3.3) with those coming from Eqs. (2.27)–(2.29). To this end, we have defined a mesh in the phase diagram spanned by the doping parameter δ and the ratio U/t of the Hubbard parameters. The meshpoints range from $\delta=0$ to 0.4 in steps of 0.1, and from $U/t=2$ to 15 in steps of 1. In Fig. 3, we have plotted the function $f(\delta,U/t)=(E_{\rm sfp}-E_{\rm sdw})\Theta(E_{\rm sdw}-E_{\rm sfp})$, where $E_{\rm sfp}$ and $E_{\rm sdw}$ are the mean-field energies of the spin-flux phase and the spin-density wave, respectively, and $\Theta(x)$ is the step function. In other words, $f(\delta,U/t)=E_{\rm sfp}-E_{\rm sdw}$ for $E_{\rm sdw}>E_{\rm sfp}$ and $f(\delta,U/t)=0$ otherwise. The corresponding contour plot in the lower part of Fig. 3 clearly identifies two regions of the parameter space, where the spin-flux phase is *energetically favored:* A first one at

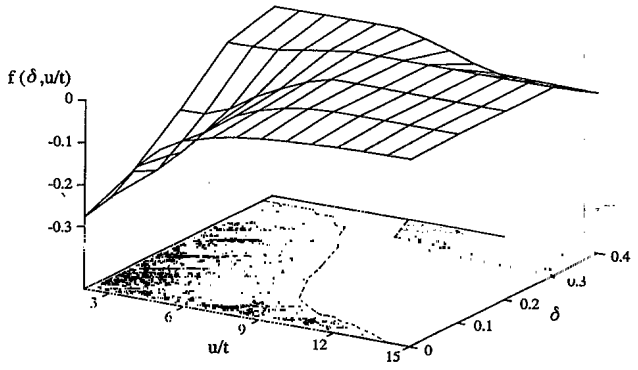

FIG. 3. The function $f(\delta,U/t)=(E_{\rm sfp}-E_{\rm sdw})\Theta(E_{\rm sdw}-E_{\rm sfp})$ versus doping δ and the ratio U/t of the Hubbard parameters. The quantities $E_{\rm sdw}$ and $E_{\rm sfp}$ refer to the mean-field energy of the spin-density wave and the spin-flux phase, respectively, and $\Theta(x)$ denotes the step function.

$U/t\approx2-10$ and $\delta\approx0-0.2$, and a second one at $U/t\approx10-15$ and $\delta\approx0.3-0.4$. Closer inspection reveals that the spin-flux phase at zero doping is actually favored for *all* values of U/t considered here, see the solid line in Fig. 4 representing the energy difference $\Delta E=E_{\rm sfp}-E_{\rm sdw}$. For finite doping $\delta=0.2$, the dotted line in Fig. 4 shows that a crossover from a sfp to a sdw ground state occurs around $U/t\approx8$, as expected from the information in Fig. 3. For a more detailed analysis, let us distinguish between the two main contributions to the mean-field energy, namely, the sum over the quasiparticle levels $E_{\rm qp}$ [the first term in Eqs. (2.27) and (3.1)] and the magnetization energy $E_k=US^2$. In Fig. 5, the upper and the lower solid curve show the behavior of $\Delta E_{\rm qp}=E_{\rm qp}^{\rm sfp}-E_{\rm qp}^{\rm sdw}$ and $\Delta E_s=E_s^{\rm sfp}-E_s^{\rm sdw}$, respectively, at zero doping, while the dotted curves correspond to the same quantities for $\delta=0.2$. The most striking feature of Fig. 5 is that we have $E_s^{\rm sfp}<E_s^{\rm sdw}$ (and hence $S_{\rm sfp}<S_{\rm sdw}$

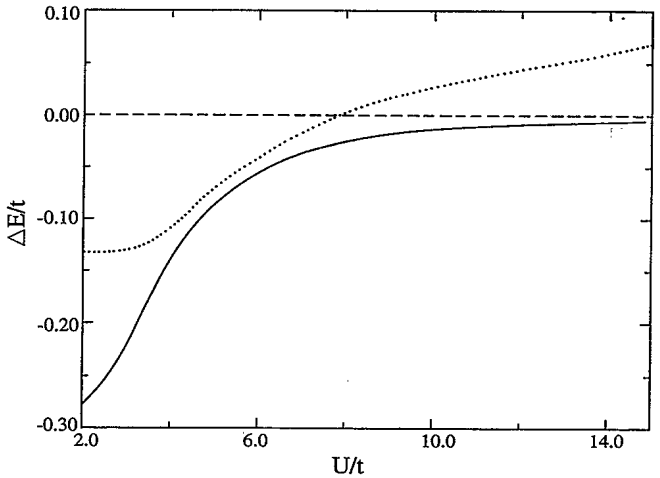

FIG. 4. The energy difference $\Delta E=E_{\rm sfp}-E_{\rm sdw}$ between the staggered spin-flux phase and the spin-density wave for $\delta=0$ (solid curve) and $\delta=0.2$ (dotted curve) as a function of U/t.

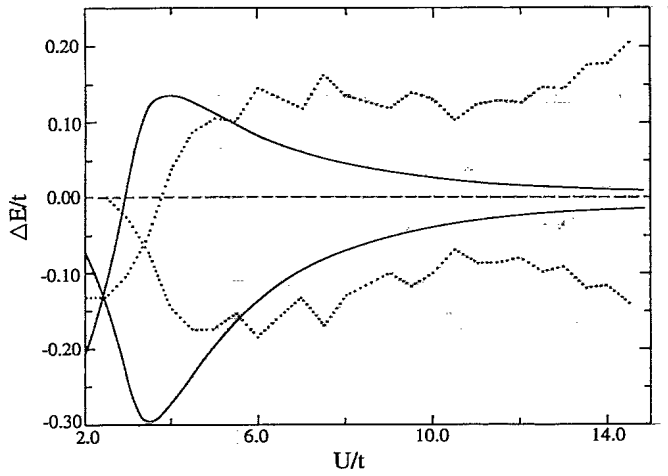

FIG. 5. The partial energy differences $\Delta E_{qp}=E_{qp}^{sfp}-E_{qp}^{sfp}$ and $\Delta E_s=E_s^{sfp}-E_s^{sfp}$ between the staggered spin-flux phase and the spin-density wave for $\delta=0$ (solid curves) and $\delta=0.2$ (dotted curves). Here, E_{qp} and E_s refer to the contributions of the quasiparticle levels and the on-site magnetization, respectively, to the mean-field energy. The curves corresponding to ΔE_s are strictly nonpositive.

for the mean-field magnetizations) for both $\delta=0$ and $\delta=0.2$ and for all values of U/t considered here. The mean-field magnetization S determines the size of the Mott-Hubbard gap in the quasiparticle excitation spectrum. The most favorable value of S is determined by two competing influences. An increase in S (and hence in the size of the gap) moves the occupied quasiparticle levels towards lower energies and, therefore, reduces the total energy of the system. On the other hand, spin alignment tends to localize the electrons due to the Pauli principle and therefore increases the total energy [cf. the term US^2 in Eqs. (2.27) and (3.1)]. In Fig. 6, a comparison of

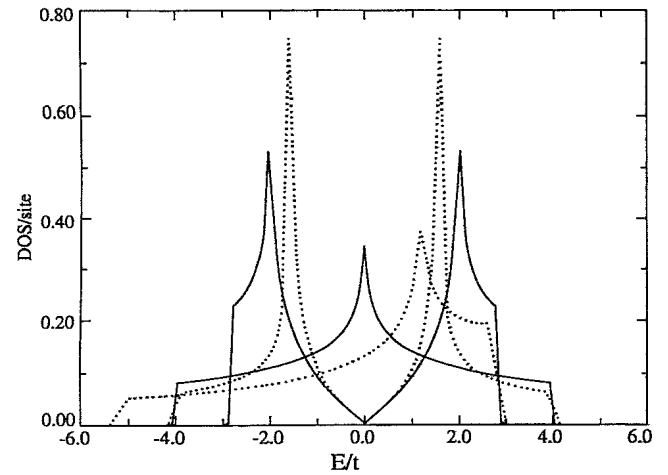

FIG. 6. Comparison between the density of states of the spin-density-wave state and the staggered spin-flux phase for $t_{nnn}/t=0$ (solid curves), and $t_{nnn}/t=0.3$ (dotted curves). We have set $S=0$, $Q_x=Q_y=\pi$. The case of the spin-density wave can be identified by the Van Hove singularity close to the band center.

the density of states for both phases considered here (solid curves, $S=0, Q_x=Q_y=\pi$) clearly shows the well-known Van Hove singularity of the usual antiferromagnetic state at the center of the band, while the density of states for the spin-flux phase vanishes at this point. These radical differences in the density of states explain why the ensuing mean-field magnetizations are so different and why, therefore, the corresponding contributions to the mean-field energy differ. Indeed, a short glance at Fig. 5 shows that the energy advantage of the spin-flux phase can be (almost) exclusively attributed to the term US^2. The sum over the quasiparticle energy levels turns out to be almost exclusively in favor of the spin-density-wave state. Over wide ranges of the parameters U/t and δ, however, this effect is overcompensated by the magnetization energy, leading to the observed overall energy advantage of this spin-flux phase. The crossover to the spin-density-wave state at finite doping is due to the fact that the energy difference ΔE_{qp} remains unusually large for increasing U/t, as compared to the case of zero doping. We are led to conclude that the spin-density-wave state—probably due to the peculiar density of states of the antiferromagnetic phase—can take better advantage of the nontrivial spiral pitch $\mathbf{Q}$ at finite values of δ.

In a next step, we investigate the stability of the situation just described under certain changes of the model. One might argue that a nearest-neighbor hopping model on a square lattice with on-site interactions is a very special case, in which the spin-density wave might be artificially handicapped (e.g., by the Van Hove singularity mentioned above). In the nearest-neighbor hopping model, there is no chirality associated with the spin-flux phase. A spin flux π is equivalent to a spin-flux $-\pi$. Furthermore, the mean-field energy of the spin-flux state is the same as that of more conventional $U(1)$ charge flux states, with the exception that a physical magnetic field is not present. We, therefore, consider the following two modifications of the original model: (i) a staggered spin-flux phase with *next-nearest*-neighbor (nnn) hopping and (ii) a *homogeneous* spin-flux phase with nnn hopping. These two cases are compared to the usual fluxless phase with nnn hopping. We restrict ourselves to the antiferromagnetic case (i.e., zero doping) in this discussion. In the homogeneous spin-flux phase every plaquette is threaded by a spin flux equal to $+\pi$. Furthermore, we assume that the spin flux is uniformly distributed over the plaquette so that the closed path $1-2-4-1$ [see Fig. 2(a)] contains a flux equal to $+\pi/2$. From the standpoint of *quantized* spin flux, this may be regarded as a mean-field state in which the quanta of spin-flux exhibit quantum-mechanical motion and are deconfined. In Figs. 2(b) and 2(c), two schemes of hopping amplitudes corresponding to the cases (i) and (ii) defined above, respectively, are indicated. In this figure, all unmarked links are associated with hopping amplitudes $+t$, links from thick lines carry $-t$, $T_1=it_{nnn}\sigma_z$, and $T_2=-it_{nnn}\sigma_z$. The second-nearest-neighbor hopping model clearly leads to distinction between π flux and $-\pi$ flux. An electron hopping across the diagonal of a plaquette experiences a spin flux of $\pi/2$, which is not equivalent to $-\pi/2$. This endows

each plaquette with a specific chirality. It also leads to a distinction between staggered and uniform spin flux. In the uniform spin-flux phase, there is a *global* chirality of the mean-field state, whereas the staggered spin-flux phase has a locally alternating chirality. As we will see, this leads to significant changes in the quasiparticle spectrum and many-electron energy. The spectrum also becomes distinct from that of the corresponding $U(1)$ charge flux states.

To determine the new mean-field energies, we have to calculate the modified quasiparticle spectra. In the case of the fluxless state, a simple calculation shows that Eq. (3.4) remains valid with ϵ_k replaced by

$$\epsilon_k' = -2t[\cos(k_x)+\cos(k_y)] - 4t_{\rm nnn}\cos(k_x)\cos(k_y) \ . \tag{3.5}$$

The analogous calculations for the models (i) and (ii) are a little more complicated. For the staggered phase (i) the mean-field Hamiltonian with antiferromagnetic background is given by

$$\tilde{H}_{\rm eff} = p_x\alpha_x + p_y\alpha_y + p_{xy}\alpha_{xy} + US\alpha_z \ , \tag{3.6}$$

where

$$p_x = -2t\cos(k_x), \quad p_y = -2t\cos(k_y) \ , \qquad p_{xy} = -4t_{\rm nnn}\cos(k_x)\cos(k_y) \ , \tag{3.7}$$

and

$$\alpha_x = -\gamma_z\tau_x, \quad \alpha_y = \gamma_x\tau_x, \quad \alpha_z = \tau_z\sigma_z \ , \qquad \alpha_{xy} = \gamma_y\tau_z\sigma_z \ . \tag{3.8}$$

The resolvent operator is simply

$$(\tilde{H}_{\rm eff}-E)^{-1} = \frac{[p_x^2+p_y^2+(US)^2-p_{xy}^2-E^2-2p_{xy}E\alpha_{xy}](p_x\alpha_x+p_y\alpha_y+US\alpha_z-p_{xy}\alpha_{xy}+E)}{[p_x^2+p_y^2+(US)^2-p_{xy}^2-E^2]^2-4p_{xy}^2E^2} \ , \tag{3.9}$$

so that the eigenvalues of $\tilde{H}_{\rm eff}$ are given by the zeros of the denominator in Eq. (3.9), i.e., by

$$E^{(i)}_{\pm\pm} = \pm[p_x^2+p_y^2+(US)^2+p_{xy}^2 \pm 2p_{xy}\sqrt{p_x^2+p_y^2+(US)^2}\,]^{1/2} \ . \tag{3.10}$$

In the case of the homogeneous flux phase (ii), the mean-field Hamiltonian formally also looks like Eq. (3.6), but now with

$$p_x = -2t\cos(k_x), \quad p_y = -2t\cos(k_y) \ , \qquad p_{xy} = -4t_{\rm nnn}\sin(k_x)\sin(k_y) \tag{3.11}$$

and

$$\alpha_x = -\gamma_z\tau_x, \quad \alpha_y = \gamma_x\tau_x, \quad \alpha_z = \tau_z\sigma_z \ , \qquad \alpha_{xy} = -\gamma_y\sigma_z \ , \tag{3.12}$$

so that

$$(\tilde{H}_{\rm eff}-E)^{-1} = \frac{[p_x^2+p_y^2+p_{xy}^2+(US)^2-E^2-2p_{xy}US\alpha_z\alpha_{xy}](p_x\alpha_x+p_y\alpha_y+US\alpha_z+p_{xy}\alpha_{xy}+E)}{[p_x^2+p_y^2+(US)^2+p_{xy}^2-E^2]^2-4p_{xy}^2(US)^2} \ , \tag{3.13}$$

and hence

$$E^{(ii)}_{\pm\pm} = \pm\sqrt{p_x^2+p_y^2+(p_{xy}\pm US)^2} \ . \tag{3.14}$$

Remarkably, repeating the calculations that led to the solid curve in Fig. 4 with the quasiparticle spectra given by Eqs. (3.5) and (3.10) and modest values of $t_{\rm nnn}$ $(0.1-0.3t)$ hardly induces any changes in Fig. 4. A glance at the corresponding density of states for $t_{\rm nnn}=0.3t$ (dotted curves in Fig. 6) shows that, indeed, the main features of the distributions are preserved. Therefore, no dramatic physical effect occurs when chiral symmetry is preserved globally.

In case (ii), however, chiral symmetry is broken globally and we encounter a different behavior. In Fig. 7, we compare the energy difference $\Delta E = E_{\rm sfp} - E_{\rm sdw}$ where "sfp" now refers to the homogeneous flux phase, for $t_{\rm nnn}=0$ (solid curve), $t_{\rm nnn}=0.2$ (dotted curve), and $t_{\rm nnn}=0.5$ (dashed curve). Obviously, the mean-field energy of the homogeneous flux phase steadily and noticeably

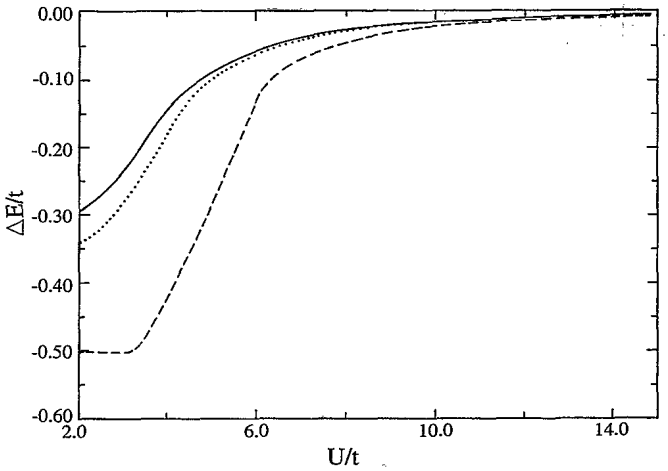

FIG. 7. The energy difference $\Delta E = E_{\rm sfp} - E_{\rm sdw}$, between the homogeneous spin-flux phase and the spin-density wave for $t_{\rm nnn}/t=0$ (solid curve), $t_{\rm nnn}/t=0.2$ (dotted curve), and $t_{\rm nnn}/t=0.5$ (dashed curve).

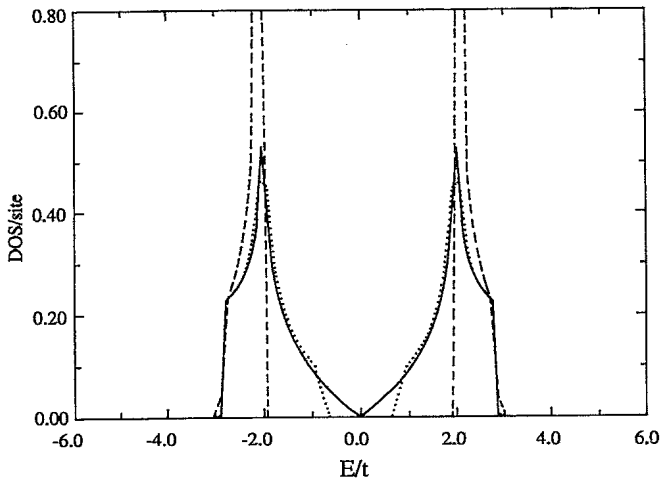

FIG. 8. The density of states of the homogeneous spin-flux phase for $S=0$, $Q_x=Q_y=\pi$, and $t_{nnn}/t=0$ (solid curve), $t_{nnn}/t=0.2$ (dotted curve), and $t_{nnn}/t=0.5$ (dashed curve).

decreases as we increase t_{nnn}. The physical reason for this effect can be read off Fig. 8, where we display the density of states corresponding to Eq. (3.14): Again, the cases $t_{nnn}=0$, $t_{nnn}=0.2$, $t_{nnn}=0.5$ correspond to the solid, dotted and dashed curve, respectively, and we have set $S=0$, $Q_x=Q_y=\pi$. Even for $S=0$ a gap in the spectrum opens as soon as $t_{nnn}\neq 0$. This appears to be an interesting observation in its own right. It indicates the possibility to have a finite gap in the quasiparticle spectrum originating from a state of broken symmetry (the homogeneous spin-flux phase), quite unlike the traditional magnetic phases.

IV. SUMMARY AND CONCLUSION

In this paper, we have given a formal motivation for the spin-flux phase introduced earlier, deriving the possibility of spin flux from a mean-field decoupling of a generalized Hubbard model with nearest-neighbor Coulomb repulsion. This procedure provides a more general framework for the spin-flux concept and the relation to the original arguments was emphasized. Two extreme cases were analyzed in depth: The spin-density wave state with zero spin-flux was compared to a spin-flux phase defined by a staggered π-flux pattern. We found that, over a wide range of the parameters U/t and δ, the latter has an energy advantage over the former. This difference in energy could be attributed to the reduced local-moment amplitude in the spin-flux phase, which was in turn a consequence of the specific changes in the density of states in the presence of spin flux. Furthermore, we found that the inclusion of moderate next-nearest-neighbor hopping did not change the picture in any essential way. Replacing the staggered by a homogeneous spin-flux pattern, however, thus breaking chiral symmetry, led to an even lower mean-field energy for nonzero next-nearest-neighbor hopping. This result could be understood by observing that the corresponding density of states exhibits a gap even for vanishing local moment amplitude.

We believe that this work provides additional plausibility that a peculiar type of correlation, as described by the spin-flux concept, may be present in the ground state of strongly interacting systems. We have shown how this possibility can formally arise and we have demonstrated that it leads, under certain conditions, to a considerable energy advantage. However, this paper is certainly only a first step. It is, in fact, necessary to determine the spin-current order parameter Δ_{ij} self-consistently. This would be particularly interesting at finite doping, where generalized spin-flux phases may be relevant. What we have shown, in this paper, is that specific configurations of spin flux on a square lattice provide an alternative to large local-moment formation, in response to nesting instability. A more exhaustive, self-consistent treatment is needed to determine the optimum combination of spin-flux and local-moment ordering. In systems, where the density of states near the Fermi energy is nonsingular, we believe that spin flux will lead only to an increase in quantum zero-point energy (as would be the case if a conventional magnetic field were applied to the system), which would not be compensated by a corresponding decrease in local-moment amplitude. This is already evident in certain doping regions in Fig. 3. Studying the behavior of the self-consistent mean-field flux value as a function of doping, should be particularly interesting. In the case of finite doping, another possibility is that correlations of the spin-flux type appear *locally* rather than *globally* and the homogeneity of the system is disrupted. This situation is more difficult to describe, as one would not only have to deal with a complicated local structure, but also with its dynamics, i.e., with the motion of locally correlated areas. It has already been pointed out in Refs. 10 and 11 that it might be ultimately possible to catch the essence of this scenario by considering a model where the flux-line singularities (associated with magnetic solitons) form a quantum liquid. One would then have to study the quantum statistical mechanics of this system. We hope to proceed along this road in a future publication.

ACKNOWLEDGMENTS

We are grateful to Andrei Golubentsev for help and advice. This work was supported by the Natural Sciences and Engineering Research Council of Canada.

[1]N. F. Mott, Proc. Phys. Soc. London Sect. A **62**, 416 (1949); Rev. Mod. Phys. **40**, 677 (1968); J. Hubbard, Proc. R. Soc. London Ser. A **276**, 238 (1963).

[2]P. W. Anderson, Science **235**, 1196 (1987).

[3]J. G. Bednorz and K. A. Müller, Z. Phys. B **64**, 189 (1986); for a review, see, *Physical Properties of High Temperature Superconductors*, edited by D. M. Ginsberg (World Scientific, Singapore, 1992), Vol. I; *Physical Properties of High Tempera-*

ture Superconductors, edited by D. M. Ginsberg (World Scientific, Singapore, 1992), Vol. II; *Physical Properties of High Temperature Superconductors,* edited by D. M. Ginsberg (World Scientific, Singapore, 1992), Vol. III.

[4]S. Uchida *et al.*, Phys. Rev. B **43**, 7942 (1991).

[5]D. B. Tanner and T. Timusk, *Physical Properties of High Temperature Superconductors III,* edited by D. M. Ginsberg (World Scientific, New York, 1992).

[6]G. A. Thomas, in *Proceedings of the 39th Scottish Universities Summer School in Physics, St. Andrews,* edited by D. P. Tunstall and W. Barford (Hilger, New York, 1991).

[7]J. D. Perkins *et al.*, Phys. Rev. Lett. **71**, 1621 (1993).

[8]C. M. Varma *et al.*, Phys. Rev. Lett. **64**, 497 (1990).

[9]P. W. Anderson, Phys. Rev. Lett. **64**, 1839 (1990).

[10]S. John and A. Golubentsev, Phys. Rev. Lett. **71**, 3343 (1993).

[11]S. John and A. Golubentsev, Phys. Rev. B **51**, 381 (1995).

[12]I. Affleck and B. Marston, Phys. Rev. B **37**, 3774 (1988); B. Marston and I. Affleck, *ibid.* **39**, 11 538 (1989).

[13]G. B. Kotliar, Phys. Rev. B **37**, 3664 (1988).

[14]G. Baskaran, Z. Zou, and P. W. Anderson, Solid State Commun. **63**, 973 (1987).

[15]F. Wilczek, Phys. Rev. Lett. **49**, 957 (1982); R. B. Laughlin, Science **242**, 525 (1988).

[16]P. Wiegmann, Prog. Theor. Phys. Suppl. **107**, 243 (1992); D. V. Khveshchenko and P. B. Wiegmann, Mod. Phys. Lett. B **3**, 1383 (1989); **4**, 17 (1990).

[17]W. E. Goff and M. B. Walker, Phys. Rev. B **45**, 12 905 (1992).

[18]E. Lieb, Phys. Rev. Lett. **73**, 2158 (1994).

[19]S. John, P. Vorganti, and W. Goff, Phys. Rev. B **43**, 13 365 (1991).